AGU PUBLICATIONS

Geochemistry, Geophysics, Geosystems

RESEARCH ARTICLE
10.1002/2017GC007247

Key Points:
- First high-resolution grain-size record in the West Philippine Sea over the past 2.36 Ma
- High-latitudes cooling drove the Equatorial Pacific SST contrast and contributed to the tropical climate changes
- A 100 kyr dominant period between 2.2 and 1.6 Myr was revealed in the ENSO-like influenced records

Supporting Information:
- Supporting Information S1
- Data Set S1

Correspondence to:
Z. Yu,
yuzhj1988@gmail.com

Citation:
Yu, Z., Wan, S., Colin, C., Song, L., Zhao, D., Huang, J., . . . Li, T. (2018). ENSO-like modulated tropical Pacific climate changes since 2.36 Myr and its implication for the Middle Pleistocene Transition. *Geochemistry, Geophysics, Geosystems*, *19*, 415–426. https://doi.org/10.1002/2017GC007247

Received 19 SEP 2017
Accepted 19 JAN 2018
Accepted article online 1 FEB 2018
Published online 15 FEB 2018

ENSO-Like Modulated Tropical Pacific Climate Changes Since 2.36 Myr and Its Implication for the Middle Pleistocene Transition

Zhaojie Yu[1,2], Shiming Wan[1,3], Christophe Colin[2], Lina Song[4], Debo Zhao[1], Jie Huang[1], Hanjie Sun[1], Zhaokai Xu[1], Anchun Li[1], and Tiegang Li[1]

[1]Key Laboratory of Marine Geology and Environment, Institute of Oceanology, Chinese Academy of Sciences, Qingdao, China, [2]Laboratoire GEOsciences Paris-Sud (GEOPS), UMR 8148, CNRS-Université de Paris-Sud, Université Paris-Saclay, Orsay Cedex, France, [3]Laboratory for Marine Geology, Qingdao National Laboratory for Marine Science and Technology, Qingdao, China, [4]Key Laboratory of Ocean Circulation and Waves, Institute of Oceanology, Chinese Academy of Sciences, Qingdao, China

Abstract El Niño/Southern Oscillation (ENSO) activity and the Pacific Walker Circulation are controlled by the zonal sea surface temperature (SST) gradient between the western and Eastern Equatorial Pacific (EEP) and the corresponding barometric difference. Variations in the zonal SST gradient since the early Pleistocene have primarily been triggered by changes in the SST in the Eastern Equatorial Pacific. However, the response of the ENSO-like long-term state to the cooling of the EEP and its coupling role with tropical Pacific climate changes are still not well established. Here we present a high-resolution grain-size record spanning the last 2.36 Myr, obtained from marine core sediment located in the West Philippine Sea in order to decipher the tropical pacific climate changes and reveal its controlling mechanism. By combining our data with other long-term climatic records from the Equatorial Pacific, we demonstrate that the cooling of SST and enhanced upwelling in the EEP resulted in the development of the Walker Circulation and increased monsoon precipitation in Luzon from 2.2 to 1.6 Myr, from 1.2 to 0.8 Myr, and since 0.2 Myr ago. The progressive cooling of the high-latitudes in the Quaternary may be responsible for our observation here. A newly identified 100 kyr dominant period between 2.2 and 1.6 Myr in the ENSO-like modulated Pacific climate records indicates that the ENSO-like system may play a key role in facilitating or responding to the global climate changes.

1. Introduction

The tropical regions play a significant role in the energy and moisture balance of modern climate system of the Earth. The temperature gradients and subsequent atmospheric pressure gradients define two atmospheric circulations: "zonal" i.e., the Walker Circulation (from the western to eastern Pacific Ocean), and "meridional," i.e., the Hadley Circulation (from tropical to subtropical regions), which largely balance the heat and moisture budgets between the tropics and extratropical areas (Wang, 2002). Variations in the intensity of these two atmospheric cells and their teleconnection might enable the tropics to initiate changes in global climate patterns in the geological past, e.g., the cooling of the Middle Pleistocene Transition (MPT) (Brierley et al., 2009; McClymont & Rosell-Melé, 2005; Pierrehumbert, 2000), but are still poorly understood. Previous studies have shown that increased zonal sea surface temperature (SST) gradients and Walker Circulation Strengthening between 1.2 and 0.8 Myr would have reduced heat flux, but would also have supplied more moisture to polar regions, which might have been responsible for the growth of the global ice sheet during the MPT (de Garidel-Thoron et al., 2005; McClymont & Rosell-Melé, 2005). Thus, in order to improve our understanding of the mechanisms involved in the tropical Pacific atmosphere-ocean system, it is crucial to determine the internal feedback processes related to global heat and moisture balances between tropical zones and the Polar Regions.

In this study, we present a high-resolution Pleistocene grain-size record (combined with an inversion algorithm for end-member modeling of grain-size compositional data) of detrital sediments from core MD06–3050 collected on the Benham Rise (Figure 1) spanning the last 2.36 Myr in order to: (i) constrain the sources

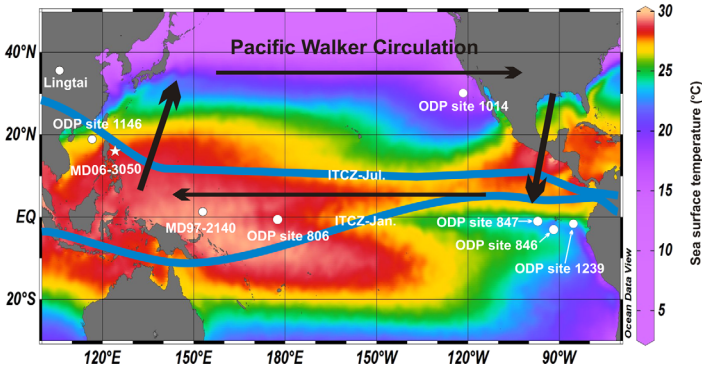

Figure 1. Pacific sites discussed in this study (core MD06–3050 in the Philippine Sea, ODP Site 1146 in the South China Sea, ODP Site 806 and core MD97–2140 in the West Pacific Ocean, and ODP Sites 846, 847, 1014, and 1239 in the East Pacific Ocean) as well as the location of Lingtai Chinese loess. Modern locations of the ITCZ in July and January are indicated by the bold blue line. Thick black lines indicate the Pacific Walker Circulation. This figure is plotted with the help of ODV4 software (Schlitzer, 2015). The temperature data was taken from the World Ocean Atlas 2013 (Zweng et al., 2013).

of different grain-size end-members and reconstruct its long-term changes; (ii) compare the monsoon records of the Southeast Asia (the West Philippine Sea and the South China Sea) and the equatorial East Pacific (EEP) climate changes (upwelling and SST records) in order to establish a link between long-term climate changes in the tropical Pacific; and (iii) explore the possible influence of internal feedback mechanisms on the tropical climate changes.

The sedimentary deposits on the Benham Rise mainly result from a complex mixture of changing percentage in sedimentary sources (eolian or fluvial supply) (Jiang et al., 2013; Wan et al., 2012; Xu et al., 2015; Yu et al., 2016), while the influences of sea-level changes and modification of the land-sea configuration are negligible. This is because the Luzon volcanic arc block the suspended materials from the East Asian Rivers (Figure 1) and the continental shelf in the west Luzon Island is very narrow and deep (average less than 10 km, the core MD06–3050 is about 230 km from the shelf with a water depth 2,967 m). The reported grain-size record and associated end-member modeling in core MD06–3050 could be used to assess the different factors that may influence detrital input on the Benham Rise. The Benham Rise in the West Philippine Sea is under the influence of the East Asian monsoon. Thus, unraveling the relative importance of eolian (winter monsoon) or fluvial supply (summer monsoon) on the Benham Rise provides an unique archive for reconstructing the intensity of East Asian summer and winter monsoon since 2.36 Myr (Wan et al., 2012; Yu et al., 2016).

2. Material and Methods

The Calypso core MD06–3050 (15°57.09′N, 124°46.77′E; water depth 2,967 m, 31.74 m in length; Figure 1) was collected in the West Philippine Sea (on the Benham Rise) during the R/V Marion Dufresne/IMAGES XIV cruise in 2006. The lithology of this core is homogeneous and is mainly brown-gray clay and nannofossil foraminifera ooze with occasional intercalated tephra layers. No obvious turbidite layers were found within core MD06–3050. The age model was established by correlating the planktonic foraminifera *G. ruber* $\delta^{18}O$ record (Sun et al., 2011) to the LR04 $\delta^{18}O$ stack line (Lisiecki & Raymo, 2005). Such age model was also verified by nine volcanic ash layers in core MD06–3050, which show parallel ages compared to the well constrained volcanic ash layers from core MD97–2143 (Ku et al., 2009).

We carefully removed the carbonate, organic matter, and biogenic opal from the detrital sediments by repeatedly using excess H_2O_2 (30% at 60°C), acetic acid (25% at 60°C), and saturated Na_2CO_3 solution (5 h at 85°C), respectively. Grain-size analyses of the terrigenous materials were carried out on a Cilas 940L apparatus in the laboratory of the Institute of Oceanology, Chinese Academy of Sciences (IOCAS), Qingdao. The measurement reproducibility is better than 2%.

End-member analysis (EMA), which estimates end-members variations based on covariability within a data set, is a powerful tool to unmix grain-size distributions into geologically meaningful end-members (Prins et al., 2000; Prins & Weltje, 1999). Utilizing the EMA method, both the grain-size distributions of each end-member and their proportions variations through time could be established and quantified. The different end-members and their variations are corresponding to: (1) different controlling mechanisms of sediment transport and/or supplied from different sources and/or (2) optional mechanisms which change systematically the grain-size distribution along the transport and deposition of the sediment from the source area (Boulay et al., 2007; Prins et al., 2000; Prins & Weltje, 1999). Such method has already been successfully used in the grain-size distribution studies in the sediments of Arabian Sea (Prins et al., 2000), Mediterranean Sea (Wu et al., 2017), North Atlantic ocean (Prins et al., 2002), and South China Sea (Boulay et al., 2007; Wan et al., 2007). Those studies applied the EMA method to identify the turbiditic, fluvial, eolian, or ice-rafted end-members based on their site character. In this study, we applied recently developed algorithms for end-member modeling of compositional data (Paterson & Heslop, 2015) to the grain-size distributions of the detrital sediment in core MD06–3050. These new algorithms, which are associated with single-

specimen unmixing techniques, represent an improvement over existing algorithms for addressing major issues in identifying grain-size subpopulations (Paterson & Heslop, 2015).

MATLAB was applied to perform continuous wavelet transform of the selected data (Figure 3). All the data were filtered with a 10–150 kyr bandpass (Duchon, 1979). All records were linearly interpolated to the average sample spacing of the record concerned. This wavelet software is available at: http://paos.colorado.edu/research/wavelets/ (Torrence & Compo, 1998). A significance level of 95% was adopted when the results are exported.

The volcanic glass particles were identified using a Philips XLSERIES XL30 scanning electron microscope (SEM) coupled with energy dispersive spectrometry (EDS) in the Laboratoire Géosciences Paris-Sud, Université de Paris-Sud in Orsay, France.

Pearson correlation analysis was perform to quantify the association between two continuous variables (e.g., between two independent variables). For two time series, X and Y, the Pearson Product Moment correlation coefficient r_{xy} was calculated as

$$r_{xy} = \frac{\sum_{i=1}^{n}(x_i - \overline{x})(y_i - \overline{y})}{(n-1)s_x s_y}$$

where n is the number of samples, and $\overline{x}$ and $\overline{y}$ are the sample means of X and Y, and S_x and S_y are the sample standard deviation of X and Y. Such method has been successfully used on the correlation analysis of paleoclimate data sets (Maher, 1998; Yan et al., 2011a).

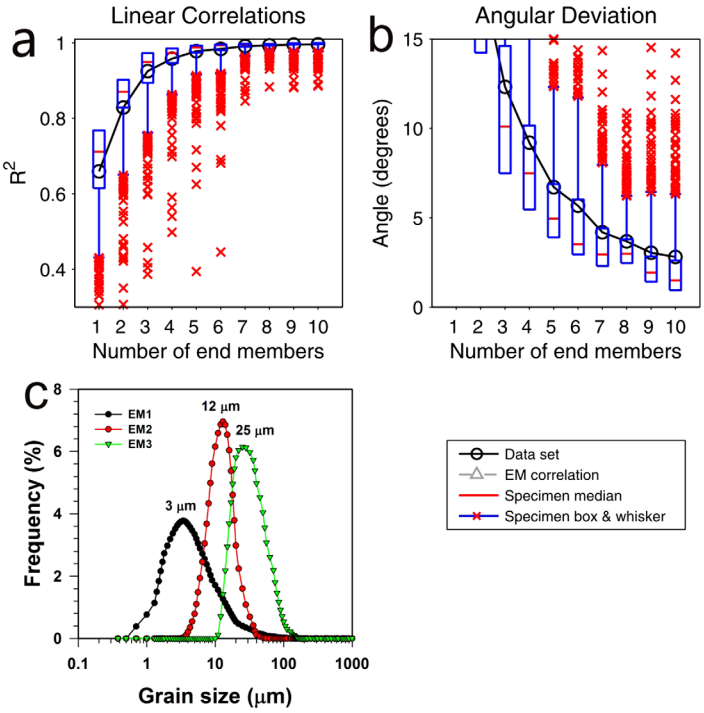

Figure 2. End-member modeling results of core MD06–3050. (a) Coefficients of determination (r^2) for each size class of models with 1–10 end-members, (b) angular differences (in degrees) between the reconstructed and observed data sets as a function of the number of end-members. The goodness of fit statistics demonstrate that the three end-member model provides the best compromise between the number of end-members and r^2 (more than 90% of the variance), and (c) modeled three end-members of the terrigenous sediment fraction of sediments from core MD06–3050.

3. Results

The lithology of core MD06–3050 is mainly clay (60–80%) and silt (10–40%), with occasional intercalated layers characterized by minor proportions of sand. End-member analysis (EMA) was applied to the 680 grain-size samples analyzed for the detrital fraction of core MD06–3050 so as to identify the number of grain-size end-members that mixed within the sediment, to reveal the grain-size distributions of different end-members and to quantify the proportion of each end-member over time (Paterson & Heslop, 2015). The goodness of fit statistics show that the three end-member model is the best optimization between the number of subpopulations and r^2 (>90% of the variance, Figures 2a and 2b). This three end-member model contains grain-size modes of ~3, ~12, and ~25 μm for end-members EM1, EM2, and EM3, respectively (Figure 2c). The proportion of EM1 varies between 20% and 80% (average of ~50%), with higher values from 2.36 to 1.6, from 1.3 to 0.5, and since 0.2 Myr ago (Figure 3). While, the proportion of EM2 (which varies from 0% to 60%, average of ~40%) is generally flat with a small decrease since 0.2 Myr ago (Figure 3). the proportion of EM3 (which varies between 0% and 80%, average of ~10%)) shows great variations, demonstrating higher values from 1.6 to 1.1 Myr and 1.0 to 0.8 Myr (Figure 3). Both the long-term variations of smectite and clay (<2 μm) percentages display similar trends comparing to that of EM1 ($r > 0.80$, $p < 0.01$) (Figure 3).

4. Discussion

4.1. Significance of the Variations in Grain Size

Previous Sr-Nd isotopic compositions and clay mineralogy studies demonstrate that detrital sediments on the Benham Rise are dominated by the mixing of terrigenous materials originating from physical erosion of soils developed above the volcanic formations of

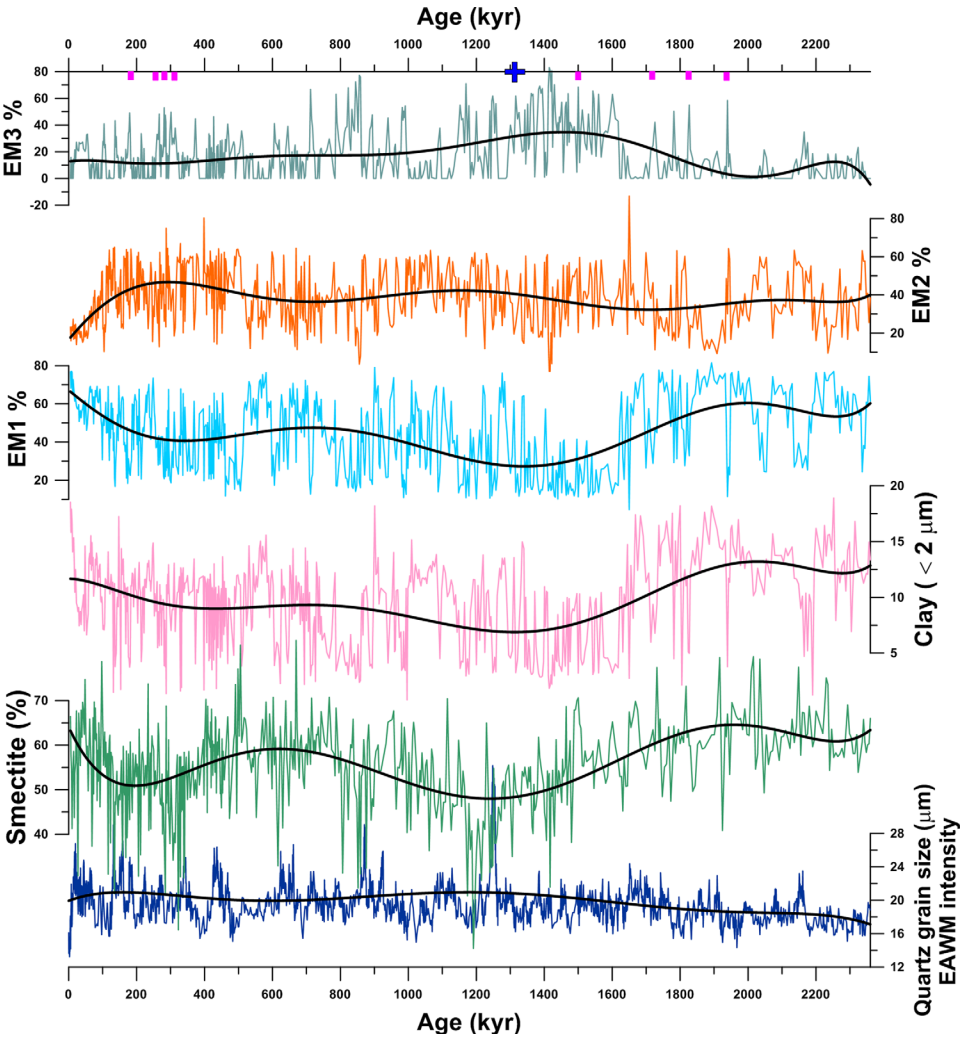

Figure 3. Relative abundances and variations of grain-size distribution (three calculated end-members and clay $< 2\ \mu m$) and smectite over the last 2.36 Myr. The mean grain size of quartz particles (MGSQ) from Lingtai loess as a proxy for East Asia Winter monsoon circulation (Sun et al., 2010) was shown for comparison. Thick black lines are straightforward polynomial fits shown to highlight general long-term trends from the original data sets. Following the method of Ku et al. (2009), nine tephra layers from core MD06–3050 were recognized by apparent color and structural changes of sediment sequence on the surface of the split core (pink squares, the blue plus indicates the layer that had been taken as an example in Figure 3 for SEM-EDS analysis). Those tephra layers are generally associated with high proportion of EM3, suggesting a direct contribution from the coarse volcanic glass particles.

Luzon Island and Chinese eolian dust (Jiang et al., 2013; Wan et al., 2012; Xu et al., 2015; Yu et al., 2016). For the mechanism of dust transport, backward trajectory analyses has shown that the particles transported to the Benham Rise can be traced back to the East Asian deserts (Jiang et al., 2013). Previous studies have shown that 10–50% (average 35%) of the terrigenous materials on the Benham Rise sediments is comprised of East Asian dust (Jiang et al., 2013; Xu et al., 2015), which is comparable with the proportion of EM2 (average 40%). In the South China Sea, EMA of detrital grain-size composition in ODP Sites 1146 and 1144 suggest that the intermediate end-member is primarily an eolian population with a diameter of about 9–11 μm, whereas the fine (about 2–5 μm) and coarse (about 19–25 μm) end-members are associated with fluvial inputs (Boulay et al., 2007; Wan et al., 2007). These conclusions for the South China Sea may be used as a reference for core MD06–3050. The eolian sourced EM2 (12 μm) in the Benham Rise is consistent with the grain-size distribution of eolian deposits of Chinese loess (peaks between 10 and 30 μm) (Sun et al., 2004; Zhang et al., 1999). This is also supported by the grain size of dust collected in Taiwan Island which reveals that more than 20% of eolian particles are around 10 μm (Hsu et al., 2009). Moreover, the evolution of EM2

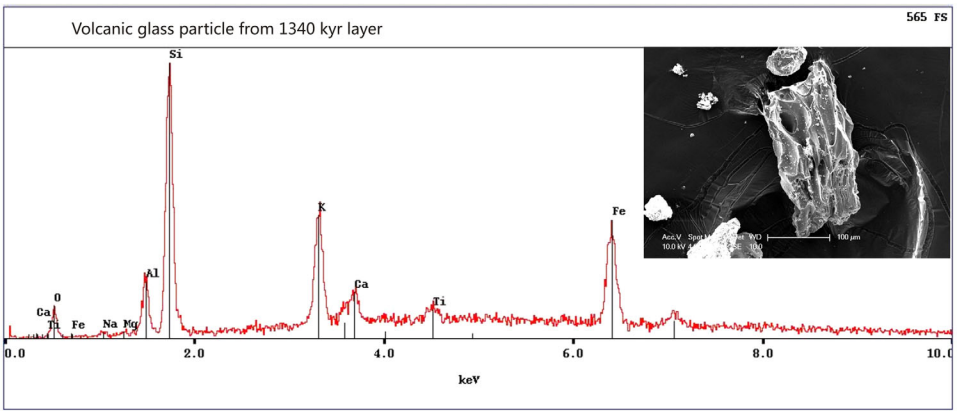

Figure 4. Typical energy dispersive spectrometry (EDS) and scanning electron microscope (SEM) image of volcanic glass particle from the tephra layers and EM3 peaks layers as shown by an example from 1,340 kyr layer. Note that the particle shows a distinct volcanic glass morphology and is rich in Si, K, Fe, Al, and Ca (Ku et al., 2009).

(12 μm) since 2.36 Myr is general flat, which is also consistent with the horizontal EAWM intensity as suggested by the mean grain size of quartz particles (MGSQ) from Lingtai loess (Sun et al., 2010). Our eolian EM2 (12 μm) does not agree with the grain size of the eolian dust in the North Pacific Ocean which shows a size mode that is slightly coarser than 2 μm, with little material coarser than 16 μm (Rea & Hovan, 1995). Such inconformity is due to the different mechanisms of eolian transportion: westerly dominated eolian dust in the North Pacific Ocean (Lim & Matsumoto, 2006; Rea & Hovan, 1995) and EAWM controlled eolian dust in the low-latitude Southeast Asia area (Qin et al., 1995; Wan et al., 2012; Xu et al., 2015).

The highest abundances of EM1 (3 μm) could be related to predominantly fluvial inputs even though eolian sources might also contribute some fine particles. This hypothesis is consistent with clay mineral sources (Wan et al., 2012; Yu et al., 2016). This fine mode in core MD06–3050 is mainly composed of clay size fraction from the weathering of volcanic formations of Luzon Island during intensive monsoon rainfall intervals. Such conclusion was confirmed by the similar variations of the smectite and clay ($<$2 μm) percentages ($r = 0.85$, $p < 0.01$) as well as the smectite and EM1 percentages ($r = 0.81$, $p < 0.01$) (Figure 3) (Yu et al., 2016). In addition, nine volcanic ash layers in core MD06–3050 (Figure 3), which show parallel ages compared to the well constrained volcanic ash layers from core MD97–2143 (Ku et al., 2009), correspond to peaks of high proportions (more than 50%) of EM3 (Figure 3). Coarse volcanic glass particles (20–100 μm) have also been identified in the tephra layers and EM3 peak layers using a scanning electron microscope (SEM) coupled with energy dispersive spectrometry (EDS) (Figure 4). The coarse material, larger than 25 μm, cannot be easily transported from Taiwanese rivers by surface current to the Benham Rise. Consequently we can hypothesize that variations in the coarse EM3 (25 μm) represent, for the most part, the coarse sediment from the Luzon Island and for the less part, the distribution of volcanic glass in the sediment of core MD06–3050. The enhancement of EASM precipitation over the Luzon Island may result in an increase in runoff and a higher input of fine end-member EM1 (mainly smectite) to the Benham Rise. The proportion of intermediate EM2 in core MD06–3050 directly corresponds to the dust inputs that are mainly controlled by the EAWM intensity (Wan et al., 2012; Yu et al., 2016). However, we cannot entirely exclude other possibilities. Our result seems inconsistent with the Sr-Nd isotopic and grain-size records from a nearby core Ph05-5, which reveal that the Asian dust contribute more in fine particles ($<$5 μm) than the moderate coarse ones (from 5 to 20 μm) (Jiang et al., 2016). Such conflict observation might be due to different local circulation and/or difference in grain-size end-member definition and Sr-Nd isotopic ranges. Further studies are encouraged to make detailed isotopic tracing efforts to determine the sediment sources (especially Sr-Nd isotopic measurements on specific grain-size end-member). Nevertheless, the ratio of fine EM1 to intermediate EM2 in core MD06–3050 can be extracted as an indicator of the relative summer versus winter monsoon intensity. Luzon Island is located on a substantially stable belt with a warm and humid climate, and its sediment erosion rate ($\sim$27 t/km^2/yr) is much lower than the lowest rate of weathering-limit conditions ($\sim$100 t/km^2/yr) (Liu et al., 2015; West, 2012). Hence, the chemical weathering of soils developed above the volcanic formations of Luzon Island can be sufficient before being transported to the ocean by the rivers

(Liu et al., 2009). In contrast to Taiwan Island, the weathering conditions on Luzon Island were mainly dominated by the erosion rate and thus by the monsoon precipitation intensity (Dadson et al., 2003; West, 2012). In addition, the two main sediment sources (Luzon Island and East Asian deserts) for core MD06–3050 are basically stable both of their geological environment and/or sediment transport in the Quaternary (Defant et al., 1989; Sun et al., 2010). Furthermore, the evolution history of EAWM intensity shows slight strengthening but roughly stable in the Quaternary (Figure 3) (Sun et al., 2010). Therefore, we argue that the evolution of the EM1/EM2 ratio in core MD06–3050 is generally dominated by the monsoon precipitation variations on the Luzon Island.

4.2. Coevolution of the Tropical Pacific Climate Changes and the ENSO-like System Since 2.36 Myr

The smectite/(illite + chlorite) ratio from core MD06–3050 was extracted as a proxy of monsoon precipitation on the Luzon Island and was coupling with the variations of ENSO-like system since 2.36 Myr ago (Yu et al., 2016). The grain-size data reported from the same core here confirms the previous conclusion and further permit us to establish the tropical climate changes (in the EEP and WEP) as a whole and further link to the cooling of the high-latitudes during the Quaternary.

Long-term evolution in the EM1/EM2 and smectite/(illite + chlorite) ratios ($r = 0.20$, $p < 0.01$ for the raw data; $r = 0.80$, $p < 0.01$ for their long-term trends) in both core MD06–3050 (Yu et al., 2016) and ODP Site 1146 (Liu et al., 2003) indicate that EASM rainfall over Southeast Asia (not only over Luzon Island) were strong from 2,360 to 1,900 kyr and subsequently by a decline from 1,900 to 1,200 kyr (Figure 5). Thereafter, the EASM precipitation intensified from 1,200 to 600 kyr, weakened from 600 to 200 kyr and increased again after 200 kyr (Figures 5a–5c).

The Pacific zonal SST gradients control the position and intensity of the Walker Circulation and subsequently affect the precipitation conditions in Southeast Asia from short to long timescales (Julian & Chervin, 1978; Lynch et al., 2015; Yan et al., 2011b; Zhang et al., 2014). El Niño-like conditions correspond to low zonal SST gradients in the tropical Pacific Ocean and weaker Walker Circulation intensity, whereas La Niña-like periods correspond to the opposite conditions. Variations of the smectite/(illite + chlorite) ratio in MD06–3050 are associated with variations in rainfall in Southeast Asia controlled by high/low zonal SST gradients induced by La Niña-/El Niño-like conditions (Yu et al., 2016). Notably, the long-term evolution of the EM1/EM2 ratio are similar to those of the smectite/(illite + chlorite) ratios in MD06–3050 and ODP Site 1146 (Liu et al., 2003), confirming their strong linkage between ENSO-like activity and climate changes in the tropical regions (Figure 5).

The long-term variations in zonal SST gradients in the tropical Pacific Ocean were mainly induced by the changes of SST in the EEP. Such SST in the EEP was primarily influenced by the temperature of the upwelling waters in the EEP (Lawrence et al., 2006). The modern upwelled waters in the EEP are principally from the mid-latitude and high-latitude and are driven by the southeast trade winds (Toggweiler et al., 1991), which in turn are mainly controlled by the latitudinal temperature difference of the Southern Hemisphere (McClymont & Rosell-Melé, 2005). Three intense upwelling periods (2.2–1.6, 1.2–0.8 Myr, and since 0.2 Myr ago) were identified by the opal MAR from the ODP Sites 846 and 847 (Farrell et al., 1995) in the EEP, which are associated with decreasing SST in ODP Site 846 (Lawrence et al., 2006) and enhanced rainfall in Southeast Asia (MD06–3050 and ODP Site 1146, Figures 5a–5c). Such conditions were accompanying with an increase in the latitudinal temperature difference in the Southern Hemisphere (indicating more intense southeast trade winds) at around 1.8 Myr as suggested by an equatorward migration of the Antarctic Circumpolar Current (Becquey & Gersonde, 2002; Diekmann & Kuhn, 2002). The diatom assemblage of ODP Site 1084 revealed intensification of Benguela upwelling and enhancement of the southeast trade winds since about 1.2 Myr (Marlow et al., 2000), which supports the enhanced upwelling from 1.2 to 0.8 Myr in the EEP (Figure 5e). Moreover, the cooling of deep waters and consequent shoaling of the thermocline in the EEP might facilitate the vertical mixing of cooler, deeper waters toward the ocean surface. This mechanism would further strengthen the sensitivity of the temperature of upwelled surface waters to the deep-water temperature (McClymont & Rosell-Melé, 2005; Philander & Fedorov, 2003). A decrease in SST of the eastern upwelling zone and development of Walker Circulation at 2 Myr ago have been attributed to cooling of mid-latitude and high-latitude sourced deep waters and subsequent thermocline shoaling in the EEP (Lear et al., 2000; Ravelo et al., 2004). Furthermore, the progressive cooling of the high-latitudes in the Quaternary (beginning in the Eocene) is likely to have played a role in both the increase of Southern Hemisphere latitudinal temperature gradient and the cooling of mid-latitude and high-latitude sourced deep waters, which

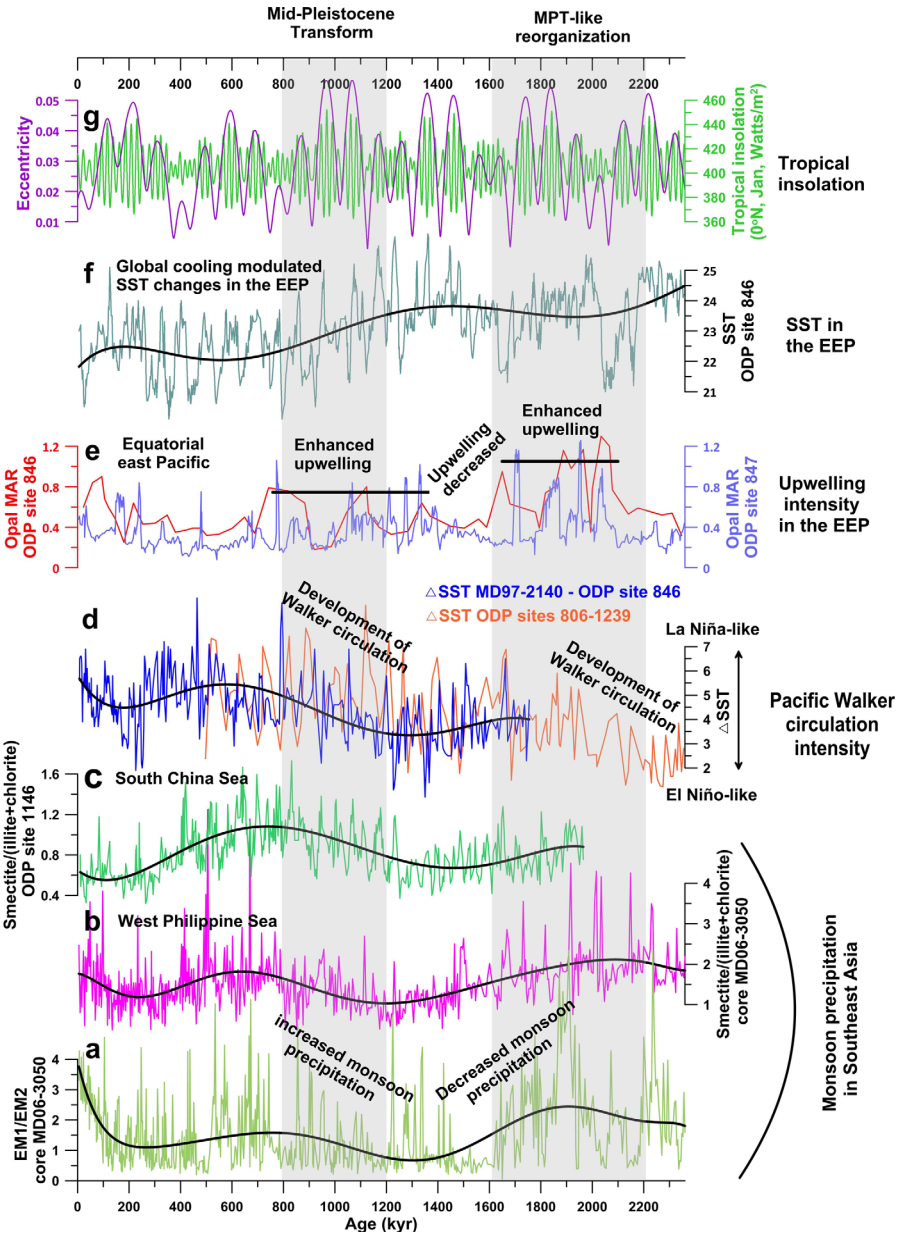

Figure 5. Comparison of climate evolution in different regions. (a) EM1/EM2 ratio from core MD06–3050 (this study), (b) smectite/(illite + chlorite) ratio from core MD06–3050 (Yu et al., 2016), (c) smectite/(illite + chlorite) ratio from ODP Site 1146 (Liu et al., 2003), (d) ΔSST, in green, corresponds to the difference between SST from core MD97–2140 and SST from core ODP 846 (de Garidel-Thoron et al., 2005), ΔSST, in brown, corresponds to the subtraction between SST from ODP Sites 806 (Wara et al., 2005) and 1239 (Etourneau et al., 2010). An El Niño-like event is generally associated with low zonal SST gradients, whereas La Niña-like conditions are exactly the reverse, (e) opal MAR from ODP Sites 846 and 847 (Farrell et al., 1995), (f) SST from ODP Site 846 (Lawrence et al., 2006), and (g) eccentricity and tropical isolation at 0°N, January (Laskar et al., 2004). Thick black lines are straightforward polynomial fits shown to highlight general long-term trends from the original data sets.

are consequently related to the increase in upwelling intensity and the decrease in deep-water temperature in the EEP (Lear et al., 2000; Zachos et al., 2001). Results obtained from core MD06–3050 indicate that monsoonal precipitation in Southeast Asia has been coupled with the tropical Pacific ENSO-like system since 2.36 Myr, and that it is sensitive to the cooling of the high-latitudes during the Quaternary. EM1/EM2 and smectite/(illite + chlorite) ratios of core MD06–3050 indicate a steep increase since 0.2 Myr ago (Figure 5). This demonstrates a La Niña-like dominate condition since 0.2 Myr ago as was also proposed

by SST and hydrological reconstruction from the western Pacific warm pool (de Garidel-Thoron et al., 2005; Zhang et al., 2016).

The intertropical convergence zone (ITCZ), which seasonally migrates toward a relative warmer hemisphere, could also influence the East Asian monsoon (Fleitmann et al., 2007; Yancheva et al., 2007) and contribute to the hydrological changes in the Southeast Asia area (including Luzon Island) from years to geological epochs (Cheng et al., 2012; Yan et al., 2015). Observations and simulation studies show that the ITCZ could migrate meridionally while its rainfall intensity changes accompanying the balance of atmospheric energy (Chiang & Bitz, 2005; Vellinga & Wood, 2002). However, the mechanisms that control the position of the ITCZ and its potential influence on the rainfall intensity in the Southeast Asia is still an unanswered question (Arbuszewski et al., 2013; Schneider et al., 2014). Moreover, there is also no reliable proxy, which indicates the paleoposition of ITCZ in the geology past. Whatever, our record from core MD06–3050 indicates a strong link between the tropical ENSO-like system and hydrological changes in the Southeast Asia area.

4.3. Implications for the MPT

The ENSO-like activity and Pacific Walker Circulation could influence both the low-latitude and mid-latitude Pacific climate variations. Although the Chinese loess Plateau is located in the mid-latitude area, an opposing variation in monsoon precipitation controlled by the tropical ENSO-like activity between northeast Asia and Southeast Asia was observed in orbital (Shi et al., 2012) and million-year timescales (Yu et al., 2016). Similarly, the opal MAR from ODP Site 1014 is a sensitive record of upwelling conditions on the Californian margin, which is tightly connected to the intensity of tropical Walker Circulation (Ravelo et al., 2004). The Wavelet analysis of the ENSO-like influenced climate records, corresponding to the rainfall record for East Asia and upwelling records for the East Pacific, display two major 100 kyr dominated periods at 2.2–1.6 Myr and after 0.8 Myr (Figure 6). However, variations in global ice volumes as reconstructed by the LR04 only show a 100 kyr fluctuation pattern starting about 0.8 Myr ago (Lisiecki & Raymo, 2005). One can therefore suggest that the Tropics may play an important role in the MPT. A high-latitude driven hypothesis involving variations in ice sheet volumes does not adequately explain the 100 kyr climate fluctuation identified in the early Pleistocene ENSO-like modulated climate records (from 2.2 to 1.6 Myr, Figures 6b–6e), at a time when the ice sheets exhibit a 41 kyr oscillation pattern (Rutherford & D'Hondt, 2000). The onset of MPT is still under debate. Most previous hypotheses explaining the MPT have invoked a high-latitude cooling origin that may be related to ice-sheet dynamics (Clark et al., 2006; Huybers & Wunsch, 2005), while recent paleoclimatic studies, in particular paleo-SST reconstructions from Equatorial Pacific Ocean, indicate that the tropics may also contribute to the onset of MPT (de Garidel-Thoron et al., 2005; McClymont & Rosell-Melé, 2005). The reason why these ENSO-like modulated records generated 100 kyr cycles in the early Pleistocene is important for understanding the MPT, but remains unclear. A shift in climate sensitivity from orbital obliquity to eccentricity/precession (Imbrie & Imbrie, 1980; Ruddiman, 2003), or an increasing nonlinearity of obliquity forcing (Liu et al., 2008) might be responsible for these observations. In any case, our study indicates for the first time that a new 100 kyr dominant period existed in the ENSO-like influenced Pacific climate records between 2.2 and 1.6 Myr (Figure 6).

Effects of tropical climate variations on high-latitudes climate can be assessed by considering the responses of the atmosphere and ocean to tropical climate changes (Ravelo et al., 2004). The shallow thermocline and cooling in the EEP could strengthen the Pacific zonal SST gradients. Subsequent atmospheric pressure difference resulting from this reinforcement of the zonal SST gradients would further strengthen the easterly trade winds and the upwelling in the EEP that would then permit a reinforcement of SST and atmospheric pressure gradients (Bjerknes, 1968; Ravelo et al., 2004). This positive feedback loop could amplify the climate perturbations in the tropics and further influence the high-latitudes climate patterns through altering the pole-ward heat and moisture transport and thus contribute to the development of more extensive ice sheets and to changes in glacial cycles, i.e., from a 41 to a 100 kyr cycle (de Garidel-Thoron et al., 2005; McClymont & Rosell-Melé, 2005; Ravelo et al., 2004). For time intervals from 2.2 to 1.6 Myr, from 1.2 to 0.8 Myr, and since 0.2 Myr ago, enhanced upwelling and a decrease in SST in the EEP were probably driven by progressively enhanced high-latitudes cooling, which indicate increased zonal SST gradients and the development of strong Walker Circulation (Figures 5f and 5g). The intensification of the Walker Circulation would lead to augmentation of rainfall in Southeast Asia, as supported by increased ratios of both EM1/EM2 and smectite/(illite + chlorite) in core MD06–3050 at these two time intervals (Yu et al., 2016). Therefore, the increased tropical zonal SST gradients and intensified Walker Circulation in the period between 1.2 and 0.8 Myr were accompanied by long-term regional hydrological changes in Southeast Asia. These changes are

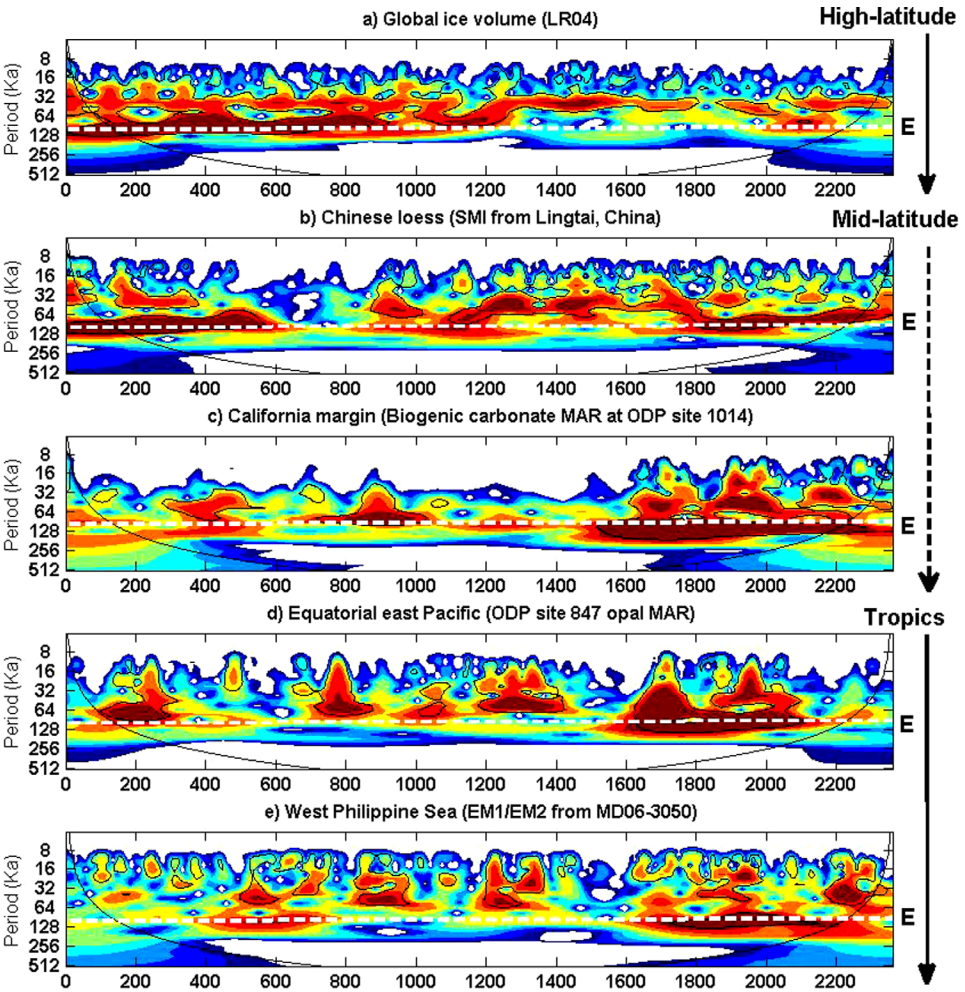

Figure 6. Wavelet power analysis for (a) stacked global benthic $\delta^{18}O$ record of LR04 (Lisiecki & Raymo, 2005), (b) summer monsoon index based on magnetic susceptibility and carbonate content from Ling tai, Chinese Loess Plateau: a proxy of monsoon rainfall (Sun et al., 2010), (c) biogenic carbonate MAR from ODP Site 1014 in the Californian margin (Ravelo et al., 2004), (d) opal MAR from ODP Site 847 in the Equatorial East Pacific (Farrell et al., 1995), and (e) EM1/EM2 ratio from core MD06–3050 (this study). Variability at the eccentricity (E) period is highlighted by the white dashed line. The solid black contour lines identify regions where spectral power meets the 5% significance level against red noise. Pale shading identifies the cone of influence where edge effects due to processing may impact upon the signal.

also indicated by sea surface salinity in this area (de Garidel-Thoron et al., 2005), implying that the intensified Walker Circulation during the 1.2–0.8 Myr period may have had a positive feedback on the MPT.

Our assumption is consistent with a sharp weakening of Atlantic Meridional Overturning Circulation (AMOC) in the early MPT as revealed by benthic stable isotope records in the Atlantic Ocean since about 1.3 Ma ago (Bell et al., 2015). This weakening would have greatly decreased the heat flux and enhanced the growth of glacial ice sheets (Bell et al., 2015). Modeling studies of tropical SST contrast and ENSO-like activity also support a tropical contribution of MPT (Rutherford & D'Hondt, 2000). We might ask ourselves why ice sheets did not also follow this 100 kyr oscillation cycle occurring in the tropics during the period between 2.2 and 1.6 Myr. We argue that this may be related to a more enhanced AMOC, on average, during this period, which would have supplied more heat to the polar regions thus limiting ice-sheet extension and maintaining the "41 kyr world" (Bell et al., 2015). Our hydrological data from WPWP, combined with other ENSO-like related records, demonstrate that both the long-term ocean cooling and the positive feedback of the ENSO-like system may have contributed to the MPT. The ENSO-like activity and Pacific Walker Circulation have driven the long-term tropical Pacific climate changes since 2.36 Myr ago and have contributed to global climate variations.

5. Conclusion

From grain-size analyses and end-member modeling, the terrigenous fraction of the detrial sediment from core MD06–3050 collected on the Benham Rise is depicted using a mixture of three end-members over the last 2.36 Ma.

The fine EM1 (mainly smectite) represents the flux of fluvial mud, which varies through time corresponding to the summer monsoon precipitation intensity. The coarse EM3 could be mainly related to the coarse fluvial sediment and volcanic glass, as also verified by SEM-EDS study. In contrast, the proportion of intermediate EM2 embodies the effect of dust inputs, which are mainly controlled by the EAWM intensity. The ratio of EM1/EM2, which obtained as a proxy of relative intensity of EASM versus EAWM, could be principally influenced by the EASM and its associated monsoon precipitation. Such conclusion is supported by a supply limited conditions on the Luzon Island and a relative stable EAWM intensity in the Quaternary.

Long-term evolution of the EM1/EM2 and smectite/(illite + chlorite) ratios in core MD06–3050 and ODP Site 1146 are generally consistent. They indicates that the EASM rainfall over Southeast Asia increased can be divided into five time intervals spanning the last 2.36 Myr: (1) a slightly increasing from 2,360 to 1,900 kyr; (2) a decline from 1,900 to 1,200 kyr; (3) an intensification from 1,200 to 600 kyr; (4) a weakened from 600 to 200 kyr; and (5) an increase again after 200 kyr. The variations of monsoon precipitation in these time intervals were further linked to the tropical Pacific climate changes, including evolution of Walker Circulation intensity (ENSO-like variations) and in particular the upwelling intensity (opal MAR from ODP Sites 846 and 847) in the EEP. Therefore, our new high-resolution grain-size results provide new insights into the temporal and spatial evolution of tropical Pacific climate changes. The high-latitude cooling is considered as a key factor that drives the long-term variations in the tropical Pacific climate changes.

Wavelet analysis of the ENSO-like influenced records in the mid-latitude (Chinese loess and California upwelling) and low-latitude (ODP Site 847 and core MD77–3050) reveal a strong 100 kyr dominant period from 2.2 to 1.6 Myr. Such result indicates that the ENSO-like records in the mid-latitude and low-latitude have prevailed 100 kyr cycle before the MPT. Therefore, the ENSO-like system probably act as a key role for the internal energy balance of the earth and further influenced the global climate change during the Quaternary.

Acknowledgments

The original data of this study are available in supporting information Table S1. We thank the crew and scientific party of the Marion Dufresne for coring the samples in the West Philippine Sea during the MD155-MARCO POLO 2 (IMAGES XIV) cruise. We thank Ana Christina Ravelo and Zhonghui Liu for their valuable comments on this manuscript. We are also grateful to Rémy Pichon for his help during the SEM-EDS analysis. Z. Yu acknowledges financial support from the CSC. This work was supported by the National Natural Science Foundation of China (41576034, 41622603, and 41376064), National Program on Global Change and Air-Sea Interaction (GASI-GEOGE-03), Strategic Science Project of CAS (XDA11030104), Innovation Project (2016ASKJ13), and Aoshan Talents Program (2017ASTCP-ES01) of Qingdao National Laboratory for Marine Science and Technology and CAS Interdisciplinary Innovation Team.

References

Arbuszewski, J. A., Demenocal, P. B., Cleroux, C., Bradtmiller, L., & Mix, A. (2013). Meridional shifts of the Atlantic intertropical convergence zone since the Last Glacial Maximum. *Nature Geoscience*, *6*(11), 959–962. https://doi.org/10.1038/ngeo1961

Becquey, S., & Gersonde, R. (2002). Past hydrographic and climatic changes in the Subantarctic Zone of the South Atlantic—The Pleistocene record from ODP Site 1090. *Palaeogeography, Palaeoclimatology, Palaeoecology*, *182*(3–4), 221–239. https://doi.org/10.1016/S0031-0182(01)00497-7

Bell, D. B., Jung, S. J., & Kroon, D. (2015). The Plio-Pleistocene development of Atlantic deep-water circulation and its influence on climate trends. *Quaternary Science Reviews*, *123*, 265–282.

Bjerknes, J. (1968). Atmospheric teleconnections from the equatorial Pacific. *Monthly Weather Review*, *97*(3).

Boulay, S., Colin, C., Trentesaux, A., Clain, S., Liu, Z., & Lauer-Leredde, C. (2007). Sedimentary responses to the Pleistocene climatic variations recorded in the South China Sea. *Quaternary Research*, *68*(1), 162–172.

Brierley, C. M., Fedorov, A. V., Liu, Z., Herbert, T. D., Lawrence, K. T., & LaRiviere, J. P. (2009). Greatly expanded tropical warm pool and weakened Hadley circulation in the early Pliocene. *Science*, *323*(5922), 1714–1718. https://doi.org/10.1126/science.1167625

Cheng, H., Sinha, A., Wang, X. F., Cruz, F. W., & Edwards, R. L. (2012). The Global Paleomonsoon as seen through speleothem records from Asia and the Americas. *Climate Dynamics*, *39*(5), 1045–1062. https://doi.org/10.1007/s00382-012-1363-7

Chiang, J. C. H., & Bitz, C. M. (2005). Influence of high latitude ice cover on the marine Intertropical Convergence Zone. *Climate Dynamics*, *25*(5), 477–496. https://doi.org/10.1007/s00382-005-0040-5

Clark, P. U., Archer, D., Pollard, D., Blum, J. D., Rial, J. A., Brovkin, V., et al. (2006). The middle Pleistocene transition: Characteristics, mechanisms, and implications for long-term changes in atmospheric pCO_2. *Quaternary Science Reviews*, *25*(23–24), 3150–3184.

Dadson, S. J., Hovius, N., Chen, H., Dade, W. B., Hsieh, M.-L., Willett, S. D., et al. (2003). Links between erosion, runoff variability and seismicity in the Taiwan Orogen. *Nature*, *426*(6967), 648–651.

de Garidel-Thoron, T., Rosenthal, Y., Bassinot, F., & Beaufort, L. (2005). Stable sea surface temperatures in the western Pacific warm pool over the past 1.75 million years. *Nature*, *433*(7023), 294–298.

Defant, M. J., Jacques, D., Maury, R. C., de Boer, J., & Joron, J.-L. (1989). Geochemistry and tectonic setting of the Luzon arc, Philippines. *Geological Society of America Bulletin*, *101*(5), 663–672.

Diekmann, B., & Kuhn, G. (2002). Sedimentary record of the mid-Pleistocene climate transition in the southeastern South Atlantic (ODP Site 1090). *Palaeogeography, Palaeoclimatology, Palaeoecology*, *182*(3–4), 241–258.

Duchon, C. E. (1979). Lanczos filtering in one and two dimensions. *Journal of Applied Meteorology*, *18*(8), 1016–1022. https://doi.org/10.1175/1520-0450(1979)018<1016:LFIOAT>2.0.CO;2

Etourneau, J., Schneider, R., Blanz, T., & Martinez, P. (2010). Intensification of the Walker and Hadley atmospheric circulations during the Pliocene-Pleistocene climate transition. *Earth and Planetary Science Letters*, *297*(1–2), 103–110.

Farrell, J. W., Raffi, I., Janecek, T. R., Murray, D. W., Levitan, M., Dadey, K. A., et al. (1995). Late Neogene sedimentation patterns in the eastern equatorial Pacific Ocean, Proceedings of the Ocean Drilling Program. *Scientific Results*, *138*, 717–756.

Fleitmann, D., Burns, S. J., Mangini, A., Mudelsee, M., Kramers, J., Villa, I., et al. (2007). Holocene ITCZ and Indian monsoon dynamics recorded in stalagmites from Oman and Yemen (Socotra). *Quaternary Science Reviews*, *26*(1–2), 170–188. https://doi.org/10.1016/j.quascirev.2006.04.012

Hsu, S. C., Liu, S. C., Arimoto, R., Liu, T. H., Huang, Y. T., Tsai, F., et al. (2009). Dust deposition to the East China Sea and its biogeochemical implications. *Journal of Geophysical Research: Atmospheres*, *114*, D15304. https://doi.org/10.1029/2008JD011223

Huybers, P., & Wunsch, C. (2005). Obliquity pacing of the late Pleistocene glacial terminations. *Nature*, *434*(7032), 491–494.

Imbrie, J., & Imbrie, J. Z. (1980). Modeling the climatic response to orbital variations. *Science*, *207*(4434), 943–953.

Jiang, F., Frank, M., Li, T., Chen, T. Y., Xu, Z., & Li, A. (2013). Asian dust input in the western Philippine Sea: Evidence from radiogenic Sr and Nd isotopes. *Geochemistry, Geophysics, Geosystems*, *14*, 1538–1551. https://doi.org/10.1002/ggge.20116

Jiang, F., Zhou, Y., Nan, Q., Zhou, Y., Zheng, X., Li, T., et al. (2016). Contribution of Asian dust and volcanic material to the western Philippine Sea over the last 220 kyr as inferred from grain size and Sr-Nd isotopes. *Journal of Geophysical Research: Oceans*, *121*, 6911. https://doi.org/10.1002/2016JC012000

Julian, P. R., & Chervin, R. M. (1978). A study of the Southern Oscillation and Walker Circulation phenomenon. *Monthly Weather Review*, *106*(10), 1433–1451.

Ku, Y. P., Chen, C. H., Song, S. R., Iizuka, Y., & Shen, J. J. S. (2009). A 2 Ma record of explosive volcanism in southwestern Luzon: Implications for the timing of subducted slab steepening. *Geochemistry, Geophysics, Geosystems*, *10*, Q06017. https://doi.org/10.1029/2009GC002486

Laskar, J., Robutel, P., Joutel, F., Gastineau, M., Correia, A., & Levrard, B. (2004). A long-term numerical solution for the insolation quantities of the Earth. *Astronomy & Astrophysics*, *428*(1), 261–285.

Lawrence, K. T., Liu, Z., & Herbert, T. D. (2006). Evolution of the eastern tropical Pacific through Plio-Pleistocene glaciation. *Science*, *312*(5770), 79–83.

Lear, C. H., Elderfield, H., & Wilson, P. (2000). Cenozoic deep-sea temperatures and global ice volumes from Mg/Ca in benthic foraminiferal calcite. *Science*, *287*(5451), 269–272.

Lim, J., & Matsumoto, E. (2006). Bimodal grain-size distribution of aeolian quartz in a maar of Cheju Island, Korea, during the last 6500 years: Its flux variation and controlling factor. *Geophysical Research Letters*, *33*, L21816. https://doi.org/10.1029/2006GL027432

Lisiecki, L., & Raymo, M. (2005). A Pliocene-Pleistocene stack of 57 globally distributed benthic $\delta^{18}O$ records. *Paleoceanography*, *20*, PA1003. https://doi.org/10.1029/2004PA001071

Liu, Z., Cleaveland, L. C., & Herbert, T. D. (2008). Early onset and origin of 100-kyr cycles in Pleistocene tropical SST records. *Earth and Planetary Science Letters*, *265*(3–4), 703–715.

Liu, Z., Trentesaux, A., Clemens, S. C., Colin, C., Wang, P., Huang, B., et al. (2003). Clay mineral assemblages in the northern South China Sea: Implications for East Asian monsoon evolution over the past 2 million years. *Marine Geology*, *201*(1–3), 133–146.

Liu, Z., Zhao, Y., Colin, C., Siringan, F. P., & Wu, Q. (2009). Chemical weathering in Luzon, Philippines from clay mineralogy and major-element geochemistry of river sediments. *Applied Geochemistry*, *24*(11), 2195–2205.

Liu, Z., Zhao, Y., Colin, C., Stattegger, K., Wiesner, M. G., Huh, C.-A., et al. (2015). Source-to-sink transport processes of fluvial sediments in the South China Sea. *Earth-Science Reviews*, *153*, 238–273.

Lynch, J., Polissar, P., Jacobel, W., Hovan, A., Pockalny, A., Lyle, M., et al. (2015). Glacial-interglacial changes in central tropical Pacific surface seawater property gradients. *Paleoceanography*, *30*, 423–438. https://doi.org/10.1002/2014PA002746

Maher, B. A. (1998). Magnetic properties of modern soils and Quaternary loessic paleosols: Paleoclimatic implications. *Palaeogeography, Palaeoclimatology, Palaeoecology*, *137*(1–2), 25–54. https://doi.org/10.1016/S0031-0182(97)00103-X

Marlow, J. R., Lange, C. B., Wefer, G., & Rosell-Melé, A. (2000). Upwelling intensification as part of the Pliocene-Pleistocene climate transition. *Science*, *290*(5500), 2288–2291.

McClymont, E. L., & Rosell-Melé, A. (2005). Links between the onset of modern Walker circulation and the mid-Pleistocene climate transition. *Geology*, *33*(5), 389–392.

Paterson, G. A., & Heslop, D. (2015). New methods for unmixing sediment grain size data. *Geochemistry, Geophysics, Geosystems*, *16*, 4494–4506. https://doi.org/10.1002/2015GC006070

Philander, S. G., & Fedorov, A. V. (2003). Role of tropics in changing the response to Milankovich forcing some three million years ago. *Paleoceanography*, *18*(2), 1045. https://doi.org/10.1029/2002PA000837

Pierrehumbert, R. T. (2000). Climate change and the tropical Pacific: The sleeping dragon wakes. *Proceedings of the National Academy of Sciences of the United States*, *97*(4), 1355–1358. https://doi.org/10.1073/pnas.97.4.1355

Prins, M. A., & Weltje, G. J. (1999). End-member modeling of siliciclastic grain-size distributions: T.he late Quaternary record of eolian and fluvial sediment supply to the Arabian Sea and its paleoclimatic significance. *Special Publications of SEPM*, *62*, 91–111.

Prins, M. A., Bouwer, L. M., Beets, C. J., Troelstra, S. R., Weltje, G. J., Kruk, R. W., et al. (2002). Ocean circulation and iceberg discharge in the glacial North Atlantic: Inferences from unmixing of sediment size distributions. *Geology*, *30*(6), 555–558.

Prins, M. A., Postma, G., Cleveringa, J., Cramp, A., & Kenyon, N. H. (2000). Controls on terrigenous sediment supply to the Arabian Sea during the late Quaternary: The Indus Fan. *Marine Geology*, *169*(3–4), 327–349.

Qin, Y., Chen, L., & Shi, X. (1995). Eolian deposition in the West Philippine Sea. *Chinese Science Bulletin*, *40*, 1595–1597.

Ravelo, A. C., Andreasen, D. H., Lyle, M., Lyle, A. O., & Wara, M. W. (2004). Regional climate shifts caused by gradual global cooling in the Pliocene epoch. *Nature*, *429*(6989), 263–267.

Rea, D. K., & Hovan, S. A. (1995). Grain-size distribution and depositional processes of the mineral component of abyssal sediments—Lessons from the North Pacific. *Paleoceanography*, *10*(2), 251–258. https://doi.org/10.1029/94PA03355

Ruddiman, W. F. (2003). Orbital insolation, ice volume, and greenhouse gases. *Quaternary Science Reviews*, *22*(15–17), 1597–1629.

Rutherford, S., & D'hondt, S. (2000). Early onset and tropical forcing of 100,000-year Pleistocene glacial cycles. *Nature*, *408*(6808), 72–75.

Schlitzer, R. (2015). Ocean data view. Retrieved from odv.awi.de

Schneider, T., Bischoff, T., & Haug, G. H. (2014). Migrations and dynamics of the intertropical convergence zone. *Nature*, *513*(7516), 45–53. https://doi.org/10.1038/nature13636

Shi, Z., Liu, X., & Cheng, X. (2012). Anti-phased response of northern and southern East Asian summer precipitation to ENSO modulation of orbital forcing. *Quaternary Science Reviews*, *40*, 30–38.

Sun, D., Bloemendal, J., Rea, D. K., An, Z., Vandenberghe, J., Lu, H., et al. (2004). Bimodal grain-size distribution of Chinese loess, and its palaeoclimatic implications. *Catena*, *55*(3), 325–340.

Sun, H., Li, T., Sun, R., Yu, X., Chang, F., & Tang, Z. (2011). Calcareous nannofossil bioevents and microtektite stratigraphy in the Western Philippine Sea during the Quaternary. *Chinese Science Bulletin*, *56*(25), 2732–2738.

Sun, Y., An, Z., Clemens, S. C., Bloemendal, J., & Vandenberghe, J. (2010). Seven million years of wind and precipitation variability on the Chinese Loess Plateau. *Earth and Planetary Science Letters*, *297*(3–4), 525–535.

Toggweiler, J., Dixon, K., & Broecker, W. (1991). The Peru upwelling and the ventilation of the South Pacific thermocline. *Journal of Geophysical Research: Oceans*, *96*(C11), 20467–20497. https://doi.org/10.1029/91JC02063

Torrence, C., & Compo, G. P. (1998). A practical guide to wavelet analysis. *Bulletin of the American Meteorological Society*, *79*(1), 61–78. https://doi.org/10.1175/1520-0477(1998)079<0061:APGTWA>2.0.CO;2

Vellinga, M., & Wood, R. A. (2002). Global climatic impacts of a collapse of the Atlantic thermohaline circulation. *Climatic Change*, *54*(3), 251–267. https://doi.org/10.1023/A:1016168827653

Wan, S., Li, A., Clift, P. D., & Stuut, J.-B. W. (2007). Development of the East Asian monsoon: Mineralogical and sedimentologic records in the northern South China Sea since 20 Ma. *Palaeogeography, Palaeoclimatology, Palaeoecology*, *254*(3–4), 561–582.

Wan, S., Yu, Z., Clift, P. D., Sun, H., Li, A., & Li, T. (2012). History of Asian eolian input to the West Philippine Sea over the last one million years. *Palaeogeography, Palaeoclimatology, Palaeoecology*, *326–328*, 152–159.

Wang, C. (2002). Atmospheric circulation cells associated with the El Niño-Southern Oscillation. *Journal of Climate*, *15*(4), 399–419.

Wara, M. W., Ravelo, A. C., & Delaney, M. L. (2005). Permanent El Niño-like conditions during the Pliocene warm period. *Science*, *309*(5735), 758–761.

West, A. J. (2012). Thickness of the chemical weathering zone and implications for erosional and climatic drivers of weathering and for carbon-cycle feedbacks. *Geology*, *40*(9), 811–814.

Wu, J., Liu, Z., Stuut, J.-B. W., Zhao, Y., Schirone, A., & de Lange, G. J. (2017). North-African paleodrainage discharges to the central Mediterranean during the last 18,000 years: A multiproxy characterization. *Quaternary Science Reviews*, *163*, 95–113. https://doi.org/10.1016/j.quascirev.2017.03.015

Xu, Z., Li, T., Clift, P. D., Lim, D., Wan, S., Chen, H., et al. (2015). Quantitative estimates of Asian dust input to the western Philippine Sea in the mid-late Quaternary and its potential significance for paleoenvironment. *Geochemistry, Geophysics, Geosystems*, *16*, 3182–3196. https://doi.org/10.1002/2015GC005929

Yan, H., Sun, L., Oppo, D., Wang, W., Liu, Y., Xie, Z., et al. (2011b). South China Sea hydrological changes and Pacific Walker Circulation variations over the last millennium. *Nature Communications*, *2*, 293.

Yan, H., Sun, L., Wang, Y., Huang, W., Qiu, S., & Yang, C. (2011). A record of the Southern Oscillation Index for the past 2,000 years from precipitation proxies. *Nature Geoscience*, *4*(9), 611. https://doi.org/10.1038/ngeo1231

Yan, H., Wei, W., Soon, W., An, Z. S., Zhou, W. J., Liu, R. M., et al. (2015). Dynamics of the intertropical convergence zone over the western Pacific during the Little Ice Age. *Nature Geoscience*, *8*(4), 315–320. https://doi.org/10.1038/ngeo2375

Yancheva, G., Nowaczyk, N. R., Mingram, J., Dulski, P., Schettler, G., Negendank, J. F., et al. (2007). Influence of the intertropical convergence zone on the East Asian monsoon. *Nature*, *445*(7123), 74–77. https://doi.org/10.1038/nature05431

Yu, Z., Wan, S., Colin, C., Yan, H., Bonneau, L., Liu, Z., et al. (2016). Co-evolution of monsoonal precipitation in East Asia and the tropical Pacific ENSO system since 2.36 Ma: New insights from high-resolution clay mineral records in the West Philippine Sea. *Earth and Planetary Science Letters*, *446*, 45–55.

Zachos, J., Pagani, M., Sloan, L., Thomas, E., & Billups, K. (2001). Trends, rhythms, and aberrations in global climate 65 Ma to present. *Science*, *292*(5517), 686–693.

Zhang, S., Li, T., Chang, F., Yu, Z., Xiong, Z., & Wang, H. (2016). Correspondence between the ENSO-like state and glacial-interglacial condition during the past 360 kyr. *Chinese Journal of Oceanology and Limnology*, *35*(5), 1018–1031.

Zhang, X. Y., Arimoto, R., & An, Z. S. (1999). Glacial and interglacial patterns for Asian dust transport. *Quaternary Science Reviews*, *18*(6), 811–819.

Zhang, Y. G., Pagani, M., & Liu, Z. (2014). A 12-million-year temperature history of the Tropical Pacific Ocean. *Science*, *344*(6179), 84–87.

Zweng, M., Reagan, J., Antonov, J., Locarnini, R., Mishonov, A., Boyer, T., et al. (2013). *World Ocean Atlas 2013, Volume 2: Salinity* (NOAA Atlas NESDIS 74, 39p.). Silver Spring, MD: National Oceanic and Atmospheric Administration.